Supplementary Information

Figure S1. X-ray photoelectron spectroscopy (XPS) scan of hollow silica microsphere. The XPS scan performed to the powder of hollow silica microsphere. Chemical composition of the materials can be calculated from the data, and their values are placed on the related peaks. Na: sodium, O: oxygen, C: carbon, Si: silicon.

Figure S2. X-ray diffraction (XRD) data of aluminum nitride and hollow silica microsphere. Hollow silica microsphere and aluminum nitride in powder form is characterized by XRD. Aluminum nitride has prominent peaks at the diffraction angles that correspond to the library values, whereas hollow silica microsphere does not have any meaningful peaks.

Figure S3. Mechanism of thermal transportation at a microscopic level for the proposed composites. After heat transfer at a macroscopic level occurs, heat flux passes through the material, passes thermal energy, and changes its temperature. It is difficult for such a flux to pass through when the composite includes hollow spheres with amorphous chemical structure, and this is emphasized by dashed blue lines. On the contrary, addition of highly conductive aluminum nitride particles creates thermal bridge, which in turn promotes heat flux to pass through.

Figure S4. Simulated thermal data of the composite layers at varied temperatures compared to pristine PDMS. Two layered materials with different chemical composition are simulated at different ambient temperatures of 0 °C, 10 °C, 25 °C, and 45 °C. The first, representing our proposed bilayer composite, is composed of (A) PDMS-aluminum nitride composite at the top and the bottom is composed of PDMS-aluminum nitride. The temperature of the interface between the two layers is 36.6 °C when the ambient temperature is 0 °C (B) The second is composed of pure PDMS to be used as a reference (i.e. control factor). The same region of interest lost thermal maintenance and dropped to 35.4 °C, denoting more than 1 °C deviation from the skin temperature.

Figure S5. Strain-stress curve of bilayer composites. (A) Experimental setup for measuring strain-stress curve. (B) Strain-stress curve of aluminum nitride composite and hollow silica composite according to ratio of each solute.

Figure S6. Thermogravimetric analysis (TGA) data of the composite layers. Weight loss measured while heating in with inert nitrogen gas, (A) PDMS-aluminum nitride composite and (B) PDMS-hollow silica microsphere composite. Loss of 3 wt% occurs at 403.9 °C and 352.2 °C for the respective composites when heated to 300 °C.

Figure S7. Differential scanning calorimetry (DSC) data of the composite layers. Latent heat measured during the second heating of A) PDMS-aluminum nitride composite and B) PDMS-hollow silica microsphere composite. No latent heat, meaning no phase change was detected in the range between −80 °C and 250 °C as there are no prominent peaks.

Figure S8. Optical cross-section images of hollow silica composite according to the deformation state. (A) The image of the composite in its normal state. The perpendicular and horizontal distances between hollow silica particle 1 (P1, green) and particle 2 (P2, blue) are denoted as X and Y with black scales, respectively. (B) The image of the composite in stretched state. The altered X and Y values are indicated with red scales. Compared to the normal state, an increase in the horizontal direction and a decrease in the vertical direction can be observed. (C) The image of the composite in compressed state. The altered X and Y values are indicated with red scales. Compared to the normal state, a decrease in the horizontal direction and an increase in the vertical direction can be observed.

Figure S9. Finite-element analysis of the inductive antenna under a horizontal strain of 10% to the entire device.

Figure S10 A graph showing response time of the device.

Figure S11. Experimental setup for durability test and the resulting graph. (A) A photo of the component submerged in a beaker of water, undergoing stirring, to verify durability and consistent thermal properties. (B) A graph of temperature recording of the device every 6 hours on the beaker. It can be confirmed that nearly identical results were obtained.

Figure S12. Result of the sensor during 24 hours of continuous attachment. Photograph of the device on a human skin and detached state every 6 hours.

Figure S13. Wireless power transfer circuitry and its characteristics. (A) Schematic top-view illustration of the device with wireless power transfer capability. (B) Circuit and block diagram of wireless power transfer device. (C) Scattering parameter comparison data between single and dual inductive antennas. The single antenna's peak frequency and power are 13.46 MHz and −11.91 dB, respectively. The dual antenna's peak frequency and power are 13.4 MHz and −8.16 dB, respectively. (D) The current output of wirelessly transferred power. TX ANT: transmitter antenna, RX ANT: receiver antenna.

Figure S14. Thermoelectric plates experimental setup. (A) The setup for thermoelectric plates experiment and (B) infrared images of upper and lower thermoelectric plates.

Figure S15. Comparison graph of commercial temperature probe and BCTS. A graph for comparison of temperature data acquired from a commercial temperature probe and BCTS. Minimal temperature variance is evident between the commercial probe and BCTS.

Figure S16. Experimental setup for comparison test between BCTS and commercial temperature probe in aquatic environment.

Figure S17. SEM and EDS imaging of hollow silica microsphere and aluminum nitride, both in powder form. Atoms are color-mapped in the images taken from the powder-form (A) hollow silica microsphere and (B) aluminum nitride. Si: silicon, O: oxygen, Na: sodium, Al: aluminum, N: nitrogen. Diameter of hollow silica microsphere on the left varies from 7.45 μm to 69.07 μm. As the aluminum nitride powders have irregular shape, longest lateral widths are measured, yielding the shortest width as 0.31 μm and the longest as 1.17 μm.

Figure S1

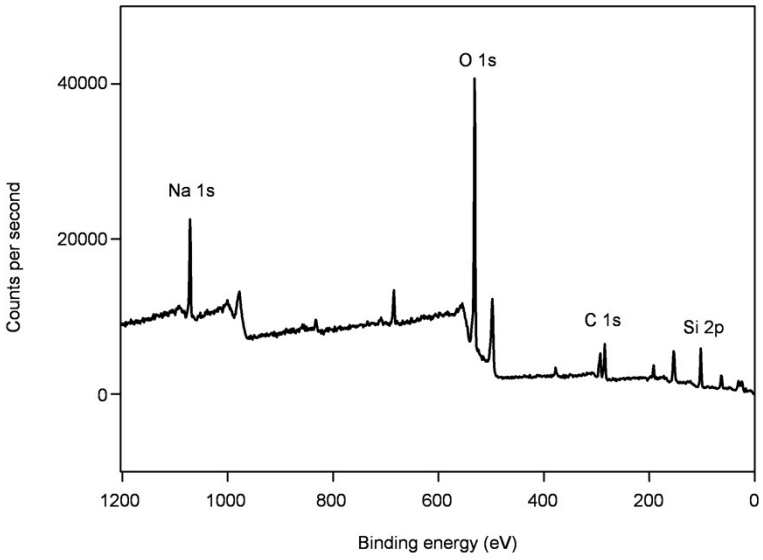
O 1s
40000
Na 1s
20000
Counts per second
C 1s
Si 2p
0
1200
1000
800
600
400
200
0
Binding energy (eV)

Figure S2

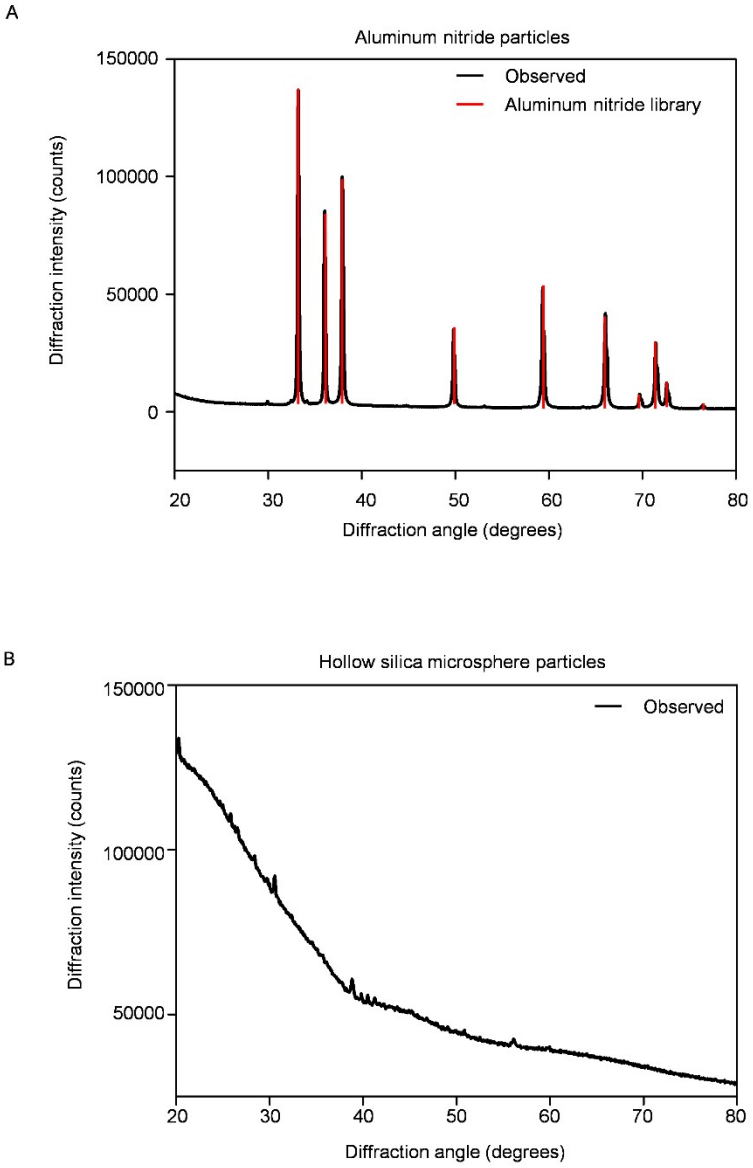
A
Aluminum nitride particles
Observed
Aluminum nitride library
Diffraction intensity (counts)
150000
100000
50000
0
20
30
40
50
60
70
80
Diffraction angle (degrees)
B
Hollow silica microsphere particles
Observed
Diffraction intensity (counts)
150000
100000
50000
20
30
40
50
60
70
80
Diffraction angle (degrees)

Figure S3

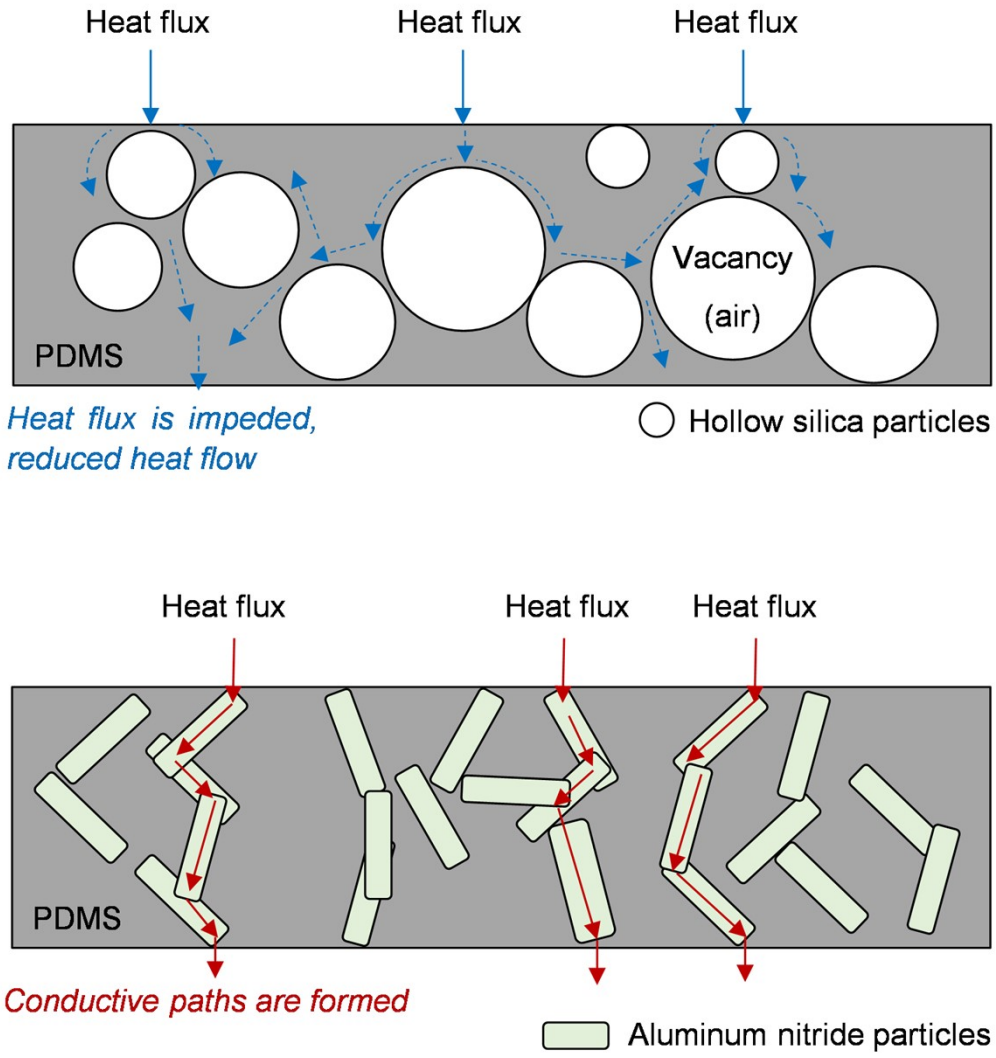
Heat flux
Heat flux
Heat flux
Vacancy
(air)
PDMS
Heat flux is impeded,
reduced heat flow
Hollow silica particles
Heat flux
Heat flux
Heat flux
PDMS
Conductive paths are formed
Aluminum nitride particles

Figure S4

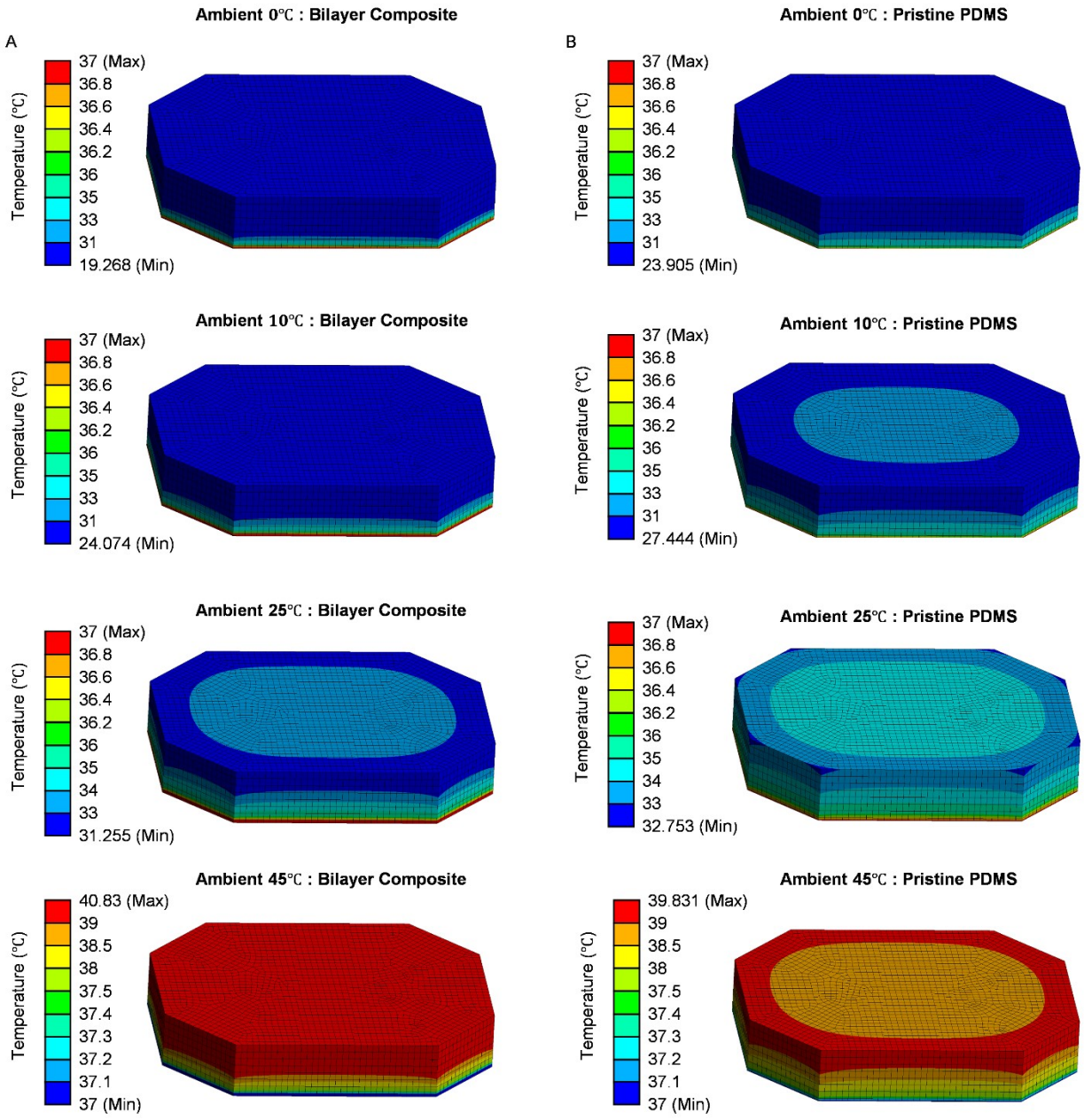
A
Ambient 0℃ : Bilayer Composite
Temperature (℃)
37 (Max)
36.8
36.6
36.4
36.2
36
35
33
31
19.268 (Min)
B
Ambient 0℃ : Pristine PDMS
Temperature (℃)
37 (Max)
36.8
36.6
36.4
36.2
36
35
33
31
23.905 (Min)
Ambient 10℃ : Bilayer Composite
Temperature (℃)
37 (Max)
36.8
36.6
36.4
36.2
36
35
33
31
24.074 (Min)
Ambient 10℃ : Pristine PDMS
Temperature (℃)
37 (Max)
36.8
36.6
36.4
36.2
36
35
33
31
27.444 (Min)
Ambient 25℃ : Bilayer Composite
Temperature (℃)
37 (Max)
36.8
36.6
36.4
36.2
36
35
34
33
31.255 (Min)
Ambient 25℃ : Pristine PDMS
Temperature (℃)
37 (Max)
36.8
36.6
36.4
36.2
36
35
34
33
32.753 (Min)
Ambient 45℃ : Bilayer Composite
Temperature (℃)
40.83 (Max)
39
38.5
38
37.5
37.4
37.3
37.2
37.1
37 (Min)
Ambient 45℃ : Pristine PDMS
Temperature (℃)
39.831 (Max)
39
38.5
38
37.5
37.4
37.3
37.2
37.1
37 (Min)

Figure S5

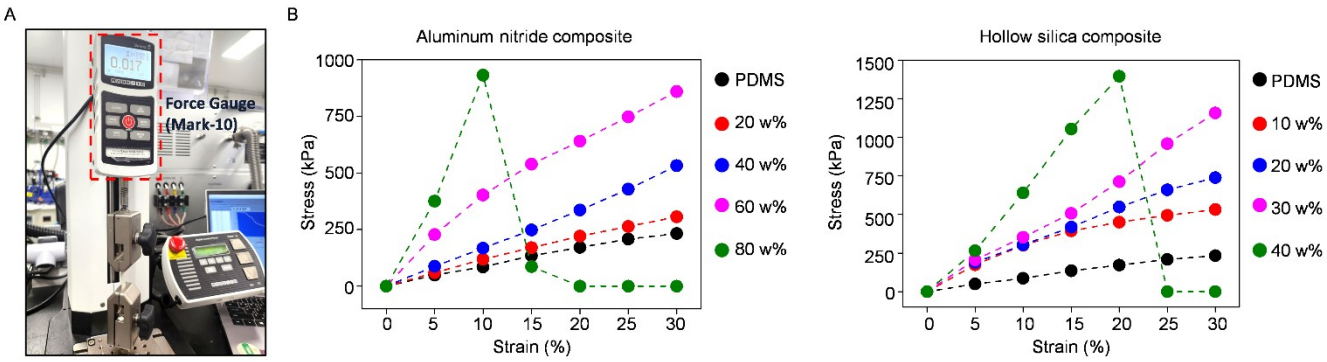
A
Force Gauge
(Mark-10)
B
Aluminum nitride composite
Stress (kPa)
Strain (%)
PDMS
20 w%
40 w%
60 w%
80 w%
Hollow silica composite
Stress (kPa)
Strain (%)
PDMS
10 w%
20 w%
30 w%
40 w%

Figure S6

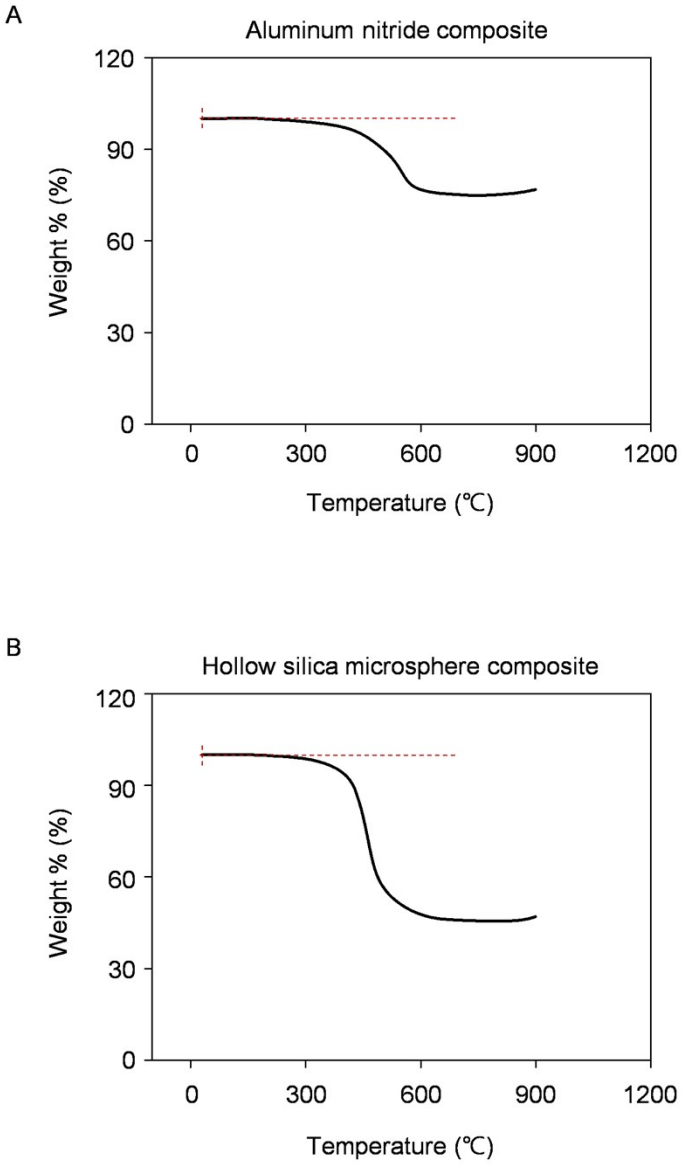
A
Aluminum nitride composite
120
90
60
30
0
Weight % (%)
0
300
600
900
1200
Temperature (℃)
B
Hollow silica microsphere composite
120
90
60
30
0
Weight % (%)
0
300
600
900
1200
Temperature (℃)

Figure S7

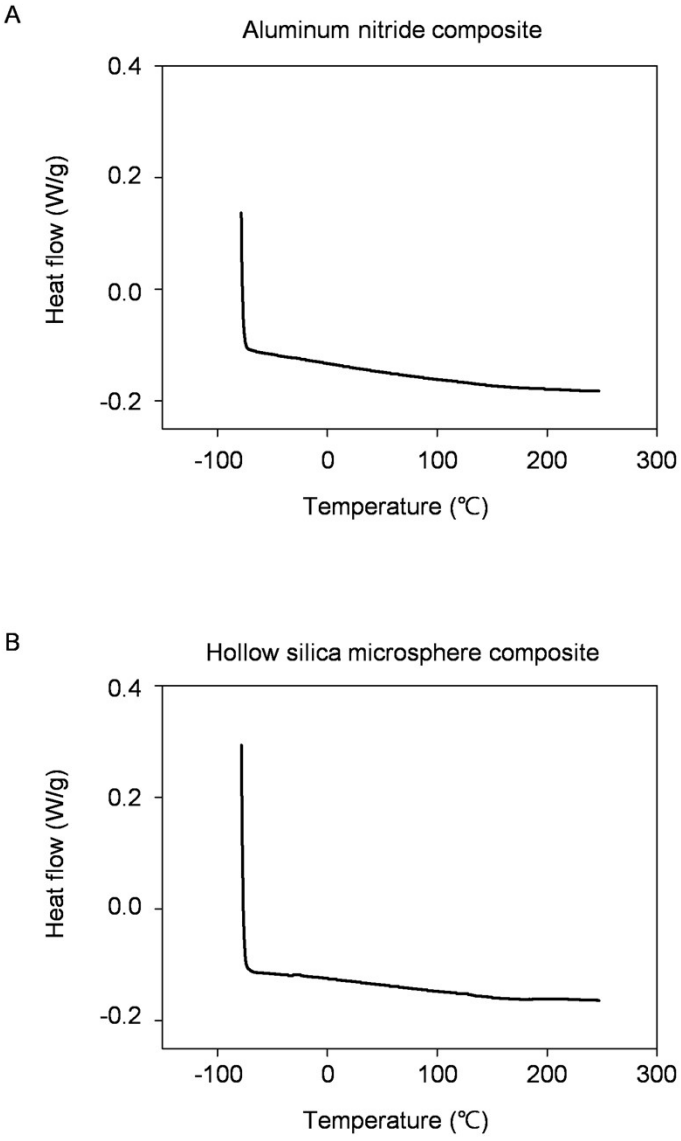
A
Aluminum nitride composite
Heat flow (W/g)
0.4
0.2
0.0
-0.2
-100
0
100
200
300
Temperature (℃)
B
Hollow silica microsphere composite
Heat flow (W/g)
0.4
0.2
0.0
-0.2
-100
0
100
200
300
Temperature (℃)

Figure S8

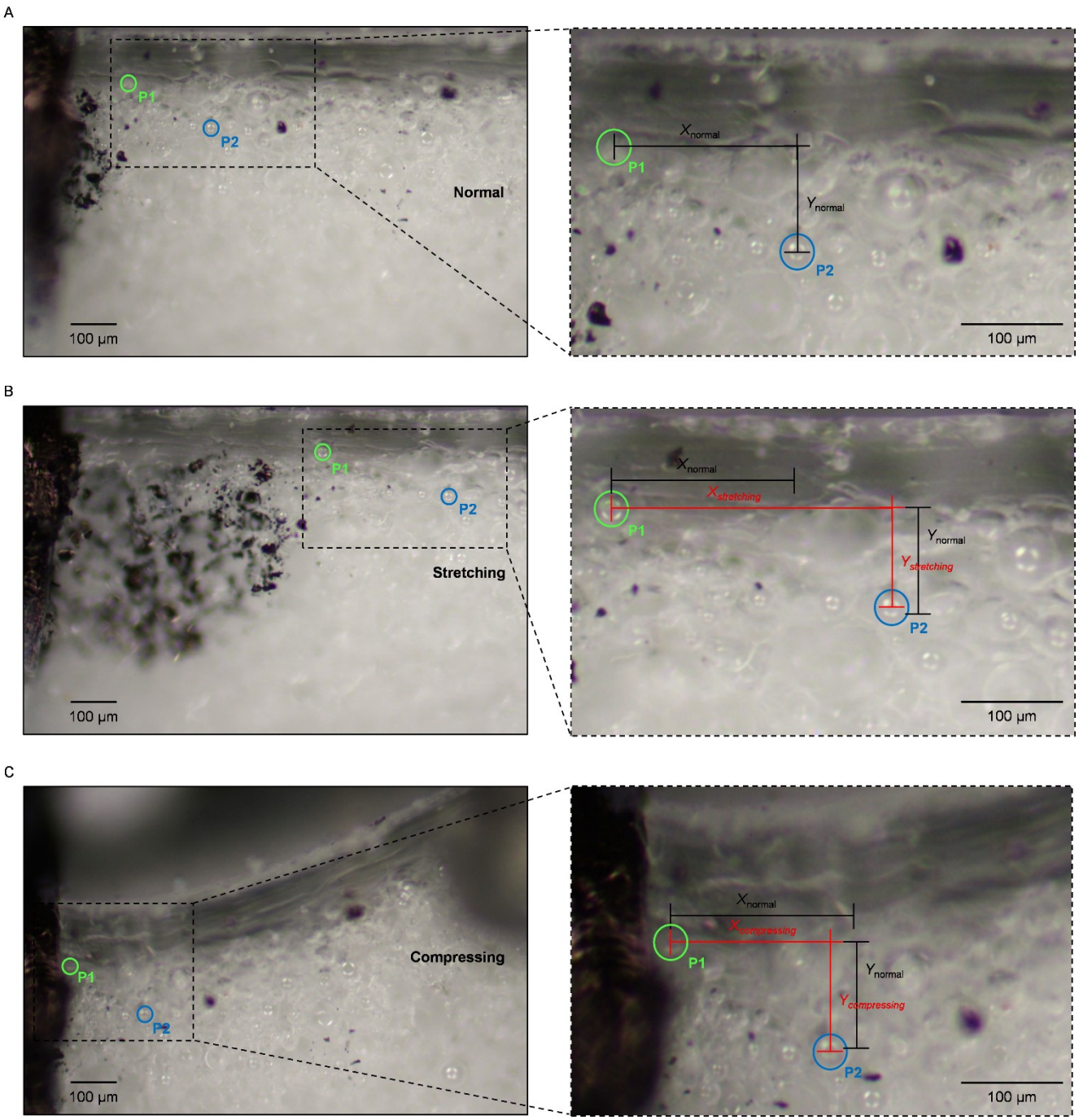
A
P1
P2
Normal
100 µm
X_{normal}
Y_{normal}
B
Stretching
$X_{stretching}$
$Y_{stretching}$
C
Compressing
$X_{compressing}$
$Y_{compressing}$

Figure S9

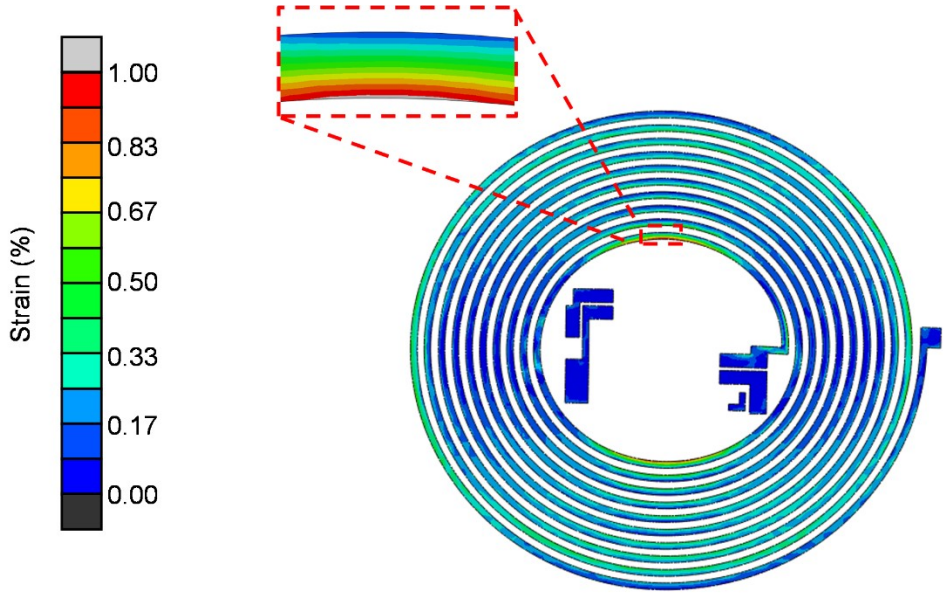

Figure S10

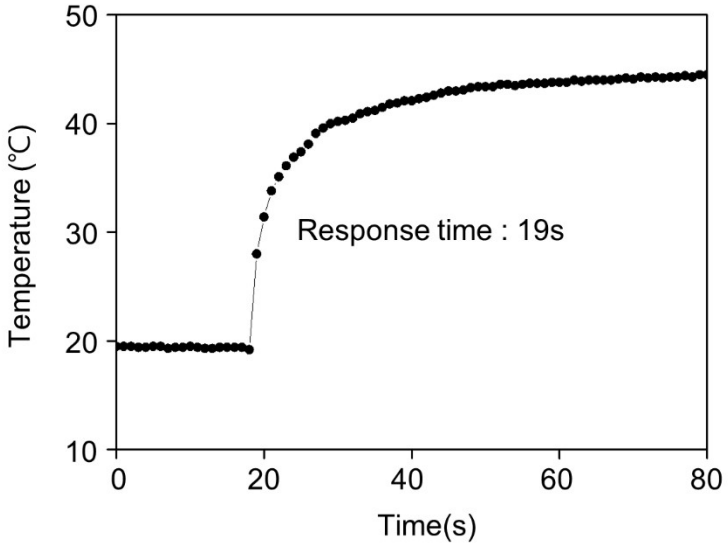
Temperature (°C)
Time(s)
Response time : 19s
50
40
30
20
10
0
20
40
60
80

Figure S11

A

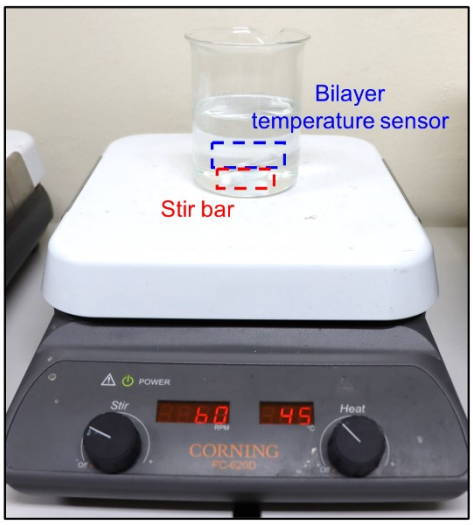

B

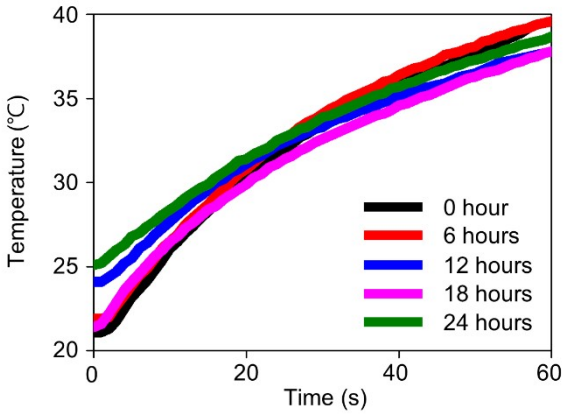

Figure S12

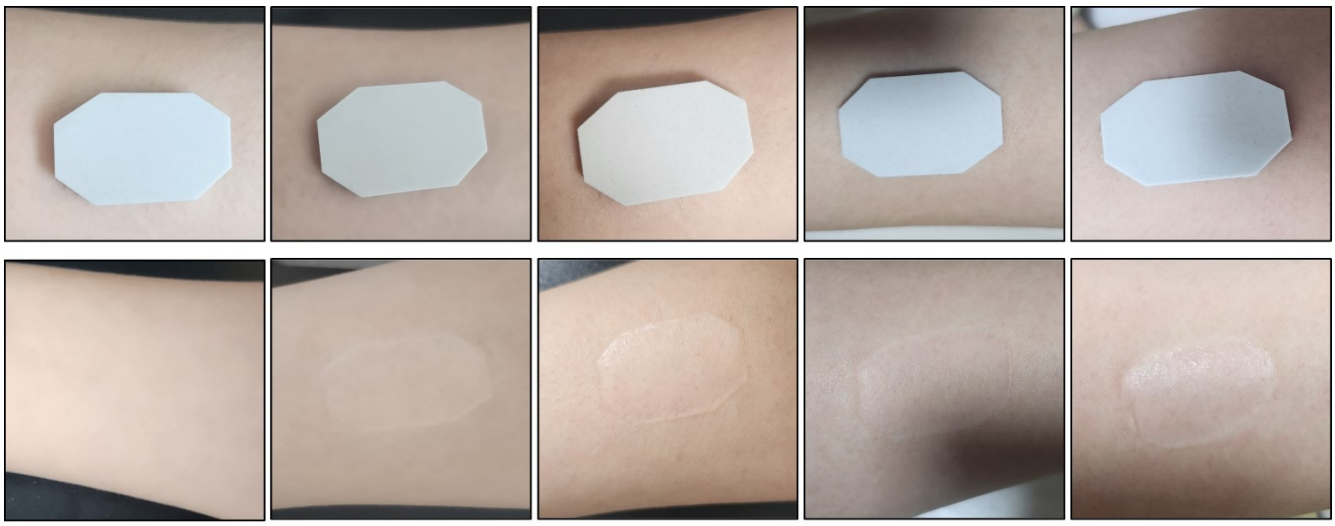

Figure S13

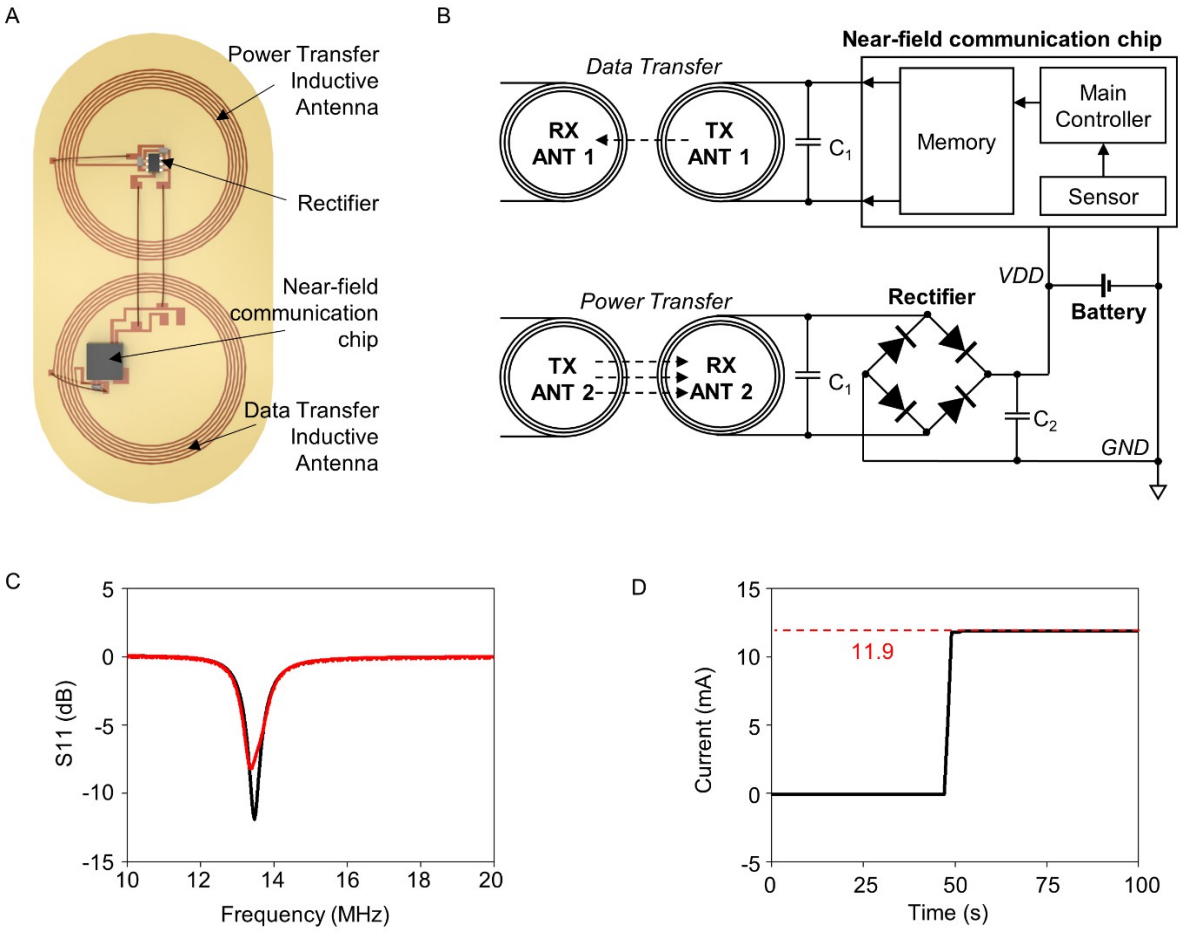
A
Power Transfer Inductive Antenna
Rectifier
Near-field communication chip
Data Transfer Inductive Antenna
B
Near-field communication chip
Data Transfer
RX ANT 1
TX ANT 1
C1
Memory
Main Controller
Sensor
VDD
Battery
Power Transfer
Rectifier
TX ANT 2
RX ANT 2
C1
C2
GND
C
S11 (dB)
Frequency (MHz)
D
11.9
Current (mA)
Time (s)

Figure S14

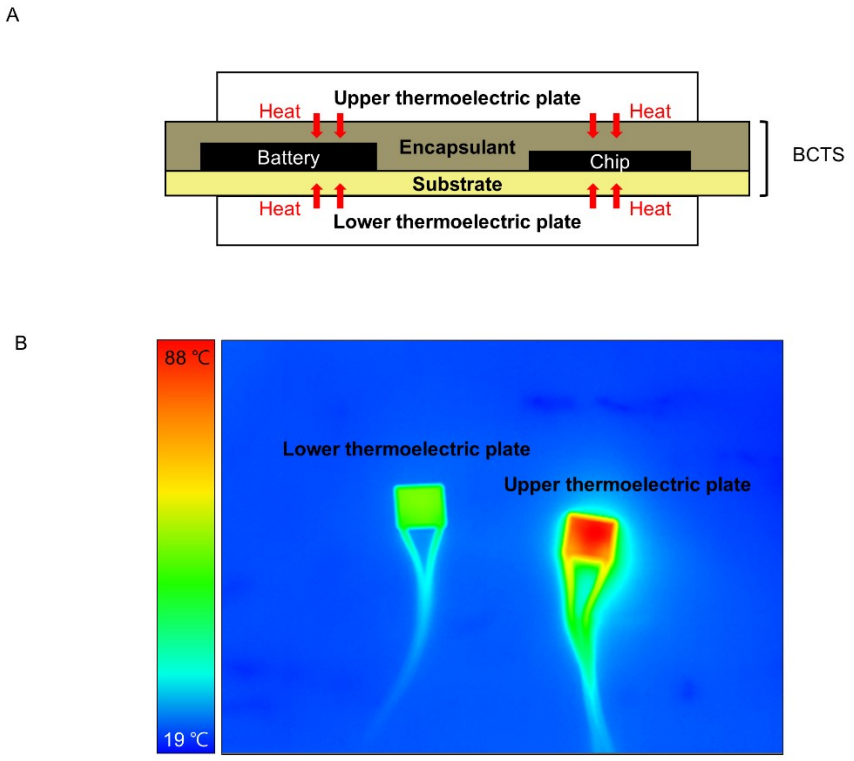
A
Upper thermoelectric plate
Heat
Heat
Battery
Encapsulant
Chip
Substrate
Heat
Heat
Lower thermoelectric plate
BCTS
B
88 ℃
19 ℃
Lower thermoelectric plate
Upper thermoelectric plate

Figure S15

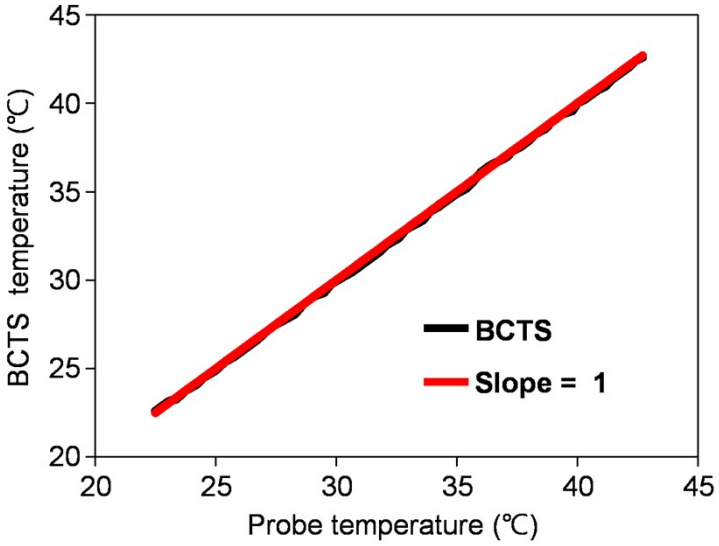
45
40
35
30
25
20
BCTS temperature (℃)
20
25
30
35
40
45
Probe temperature (℃)
BCTS
Slope = 1

Figure S16

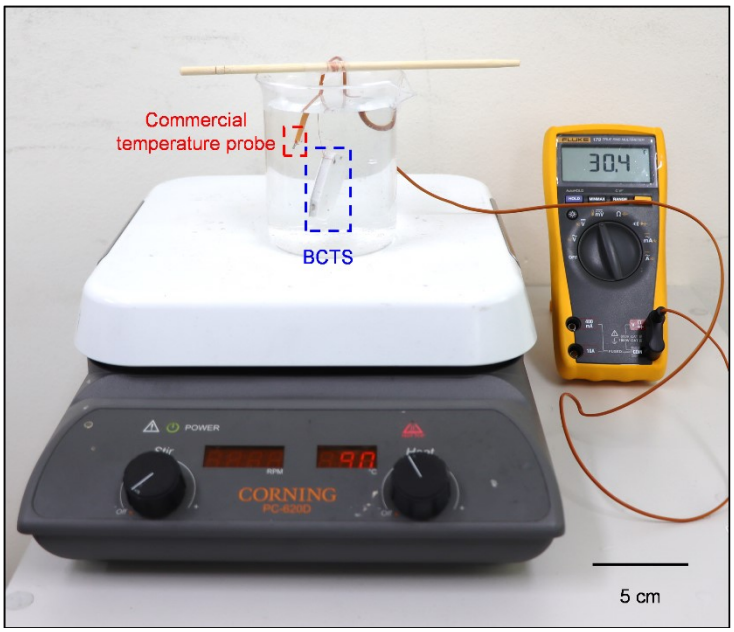

Figure S17